

Effective Three-Body Interactions in Cs($6s$)-Cs(nd) Rydberg Trimers

Christian Fey,^{1,2} Jin Yang,³ Seth T. Rittenhouse,⁴ Fabian Munkes,³ Margarita Baluktsian,³
Peter Schmelcher,^{1,5} H. R. Sadeghpour,² and James P. Shaffer³


¹Zentrum für Optische Quantentechnologien, Fachbereich Physik, Universität Hamburg,
Luruper Chaussee 149, 22761 Hamburg, Germany

²ITAMP, Harvard-Smithsonian Center for Astrophysics 60 Garden Street, Cambridge, Massachusetts 02138, USA

³Homer L. Dodge Department of Physics and Astronomy, The University of Oklahoma, Norman, Oklahoma 73072, USA

⁴Department of Physics, The United States Naval Academy, Annapolis, Maryland 21402, USA

⁵The Hamburg Centre for Ultrafast Imaging, Universität Hamburg, Luruper Chaussee 149, 22761 Hamburg, Germany

 (Received 26 March 2018; revised manuscript received 1 October 2018; published 11 March 2019)

Ultralong-range Rydberg trimer molecules are spectroscopically observed in an ultracold gas of Cs($nd_{3/2}$) atoms. The anisotropy of the atomic Rydberg state allows for the formation of angular trimers, whose energies may not be obtained from integer multiples of dimer energies. These nonadditive trimers coexist with Rydberg dimers. The existence of such effective three-body interactions is confirmed with the observation of asymmetric line profiles and interpreted by a theoretical approach that includes relativistic spin interactions. Simulations of the observed spectra with and without angular trimer lines lend convincing support to the existence of effective three-body interactions.

DOI: [10.1103/PhysRevLett.122.103001](https://doi.org/10.1103/PhysRevLett.122.103001)

Ultralong-range Rydberg molecules (ULRM) form when a Rydberg electron scatters from a ground state atom within the Rydberg orbit [1–3]. These molecules are interesting for their striking features, such as an exotic binding mechanism, huge sizes (~ 100 nm), and large permanent electric dipole moments (\sim kilo-Debyes) [4], as well as for quantum many-body phenomena at high densities [5–11]. Following the original prediction of ultralong-range Rydberg diatomic molecules [1], theoretical work predicted the formation of polyatomic ULRM where on average more than one perturber is bound within the Rydberg electron orbit [12,13]. It is appropriate to distinguish these molecules by the angular momentum l of the Rydberg electron. Triatomic molecules with $l=0$ were observed shortly after the initial discovery of diatomic ULRM [14]. Additionally, observations of similar and higher order Rb and Sr Rydberg oligomers have been reported [5,7,10,15]. Since the Rydberg electron is in an isotropic s -state, the interactions among the nuclei are additive and the binding energies are always integer multiples of the dimer energies.

In this work, we report on the observation of a new class of ultralong-range Rydberg molecules that form primarily due to the intrinsic anisotropy of Cs(nd) Rydberg wave functions; see Fig. 1. These Rydberg trimer states appear in the experiment red detuned from the atomic lines, when Cs atoms are photoexcited into $nd_{3/2}$ Rydberg states. Computations of Born-Oppenheimer (BO) potential energy surfaces (PES) enable us to simulate theoretical line profiles for dimer and trimer signals, which are compared to the experimental spectra and lend support to the

existence of nonadditive effective three-body interactions in the molecular Hamiltonian. A crucial aspect of the observed three-body spectral profile is the influence of relativistic spin-orbit and hyperfine interactions that lift the underlying degeneracy in the nonrelativistic molecular Hamiltonian. Strong support for our interpretation is found in the simulated spectra that include only dimer states vs the spectra that combine dimer and trimer states. These non-additive trimers coexist with Rydberg dimer lines.

The formation of Rydberg trimers whose energies are *not* combinatorially derived from dimer energies is a bound molecular realization of an effective three-body interaction whose existence is not manifest in pairwise interactions. Effective three-body potentials, as products of two-body interactions, have been phenomenologically derived from the vibrational spectra of alkali metal trimers [16]. Three-body and higher multibody interactions appear in various models for many-body condensed matter and quantum information Hamiltonians, including the quantum loop models describing topological order with four spins [17], adiabatic quantum computing Hamiltonians [18], and perturbation gadget Hamiltonians [19]. Effective three-body Hamiltonians have been proposed in atomic and molecular systems with polar molecules in optical lattices [20], for three interacting bosons near a two-body Feshbach resonance [21], with optical lattice modulation [22], and circuit QED systems [23]. Three-body Förster resonances, where two-body resonances are absent, were recently observed in Rydberg excitation in an ultracold Rb gas [24,25].

In its simplest manifestation, the interaction of a Rydberg electron at position \mathbf{r} and spin s_r with two ($i = 1, 2$) ground

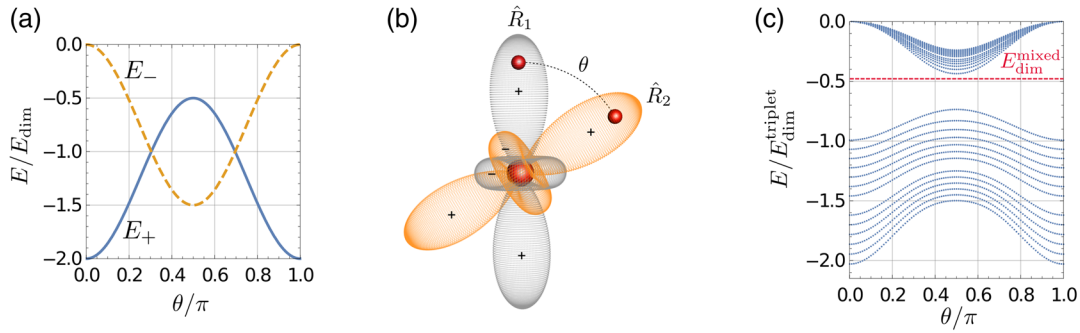


FIG. 1. The angular trimer potential energy curves (a) for $R_1 = R_2 = 1868 a_0$ for excitation into the Cs($34d_{3/2}$) Rydberg state, without any spin-dependent terms in the interaction Hamiltonian, i.e., E_{\pm} terms in Eq. (2) rescaled by $E_{\text{dim}}(R = 1868 a_0)$. The primitive orbitals (signs indicated) whose superpositions $\psi_{\pm}(\mathbf{r}; \mathbf{R}_1; \mathbf{R}_2)$ produce the eigenvalues E_{\pm} , are illustrated in (b). The angular configuration of the Rydberg core (at the origin) and the two ground state atoms (unit vectors \hat{R}_1, \hat{R}_2) are represented by the central sphere and the outer spheres, respectively. In (c) the relativistic spin-dependent interactions deform the curves E_{\pm} and lift degeneracies, leading to modified angular potentials. Here $E_{\text{dim}}^{\text{triplet}} = 71$ MHz ($E_{\text{dim}}^{\text{mixed}} = 34$ MHz) corresponds to the energy at the minimum of the outermost well of the triplet dominated (mixed singlet or triplet) dimer PES; see the dashed blue (red) curve in Fig. 2.

state alkali metal atoms at positions \mathbf{R}_i and spins s_i can be described by a Fermi pseudopotential [26]. In atomic units and for pure s -wave scattering, this interaction potential is given by $\hat{V} = \hat{V}_1 + \hat{V}_2$, where

$$\hat{V}_i = 2\pi\delta(\mathbf{r} - \mathbf{R}_i)[a_s^S(k_i)\hat{P}_i^S + a_s^T(k_i)\hat{P}_i^T]. \quad (1)$$

The operators $\hat{P}_i^{S(T)}$ project independently onto the singlet (S) and triplet (T) spin channels of the two alkali metal atoms, where $\hat{P}_i^T = s_r \cdot s_i + 3/4$ and $\hat{P}_i^S = 1 - \hat{P}_i^T$. The interaction strength in each channel is determined by the singlet (triplet) s -wave scattering length $a_s^{S(T)}(k_i)$ for a ground state atom and a free electron with momentum k_i .

When a ground state atom lies within the Rydberg electron cloud, the contact potential perturbs the Rydberg energy levels and leads to oscillatory PES [1,2]. These PES are depicted in Fig. 2 for a Cs($34d_{3/2}$) Rydberg electron where only the first ground state atom (hyperfine state $F_1 = 3$) is present, i.e., $R_2 \rightarrow \infty$ and $R = R_1$. For large distances, $R > 1800 a_0$ with a_0 being the Bohr radius, one finds a set of deep potentials (dashed blue line) with almost pure electronic triplet character and a set of shallow potentials (dashed red line) with mixed singlet or triplet character [27,28]. This spin mixing results from the interplay of three competing interactions: the Fermi pseudopotential, the Rydberg electron spin-orbit coupling, and the ground state atom hyperfine interactions. Vibrational dimer states bound in the outer wells (similar to the colored solid lines) have been confirmed experimentally [28–31]. At distances $R < 1800 a_0$, additional p -wave interactions become important [32–34]. They lift the degeneracy of the potentials and lead to sharp drops at distances where the Rydberg electron p -wave scattering phase shifts are resonant. These effects are described in more detail in [35].

When two ground state atoms lie within the electronic Rydberg cloud, the PES depend on R_1, R_2 and the enclosed angle θ ; see Fig. 1. In the absence of all spin interactions, analytical expressions for PES can be derived. This has been demonstrated for triatomic trilobites [12,13,36] as well as for triatomic low-angular momentum states [37]. For $R_1 = R_2$, the $l = 2$ trimer eigenstates can be expressed as linear combinations $\psi_{\pm}(\mathbf{r}; \mathbf{R}_1; \mathbf{R}_2) = \mathcal{N}_{\pm}(\mathbf{R}_1, \mathbf{R}_2)[\psi_{\text{dim}}(\mathbf{r}; \mathbf{R}_1) \pm \psi_{\text{dim}}(\mathbf{r}; \mathbf{R}_2)]$ of the dimer eigenstates $\psi_{\text{dim}}(\mathbf{r}; \mathbf{R}) = \sum_m \phi_{n,l=2,m}(\mathbf{R})^* \phi_{n,l=2,m}(\mathbf{r})$, with

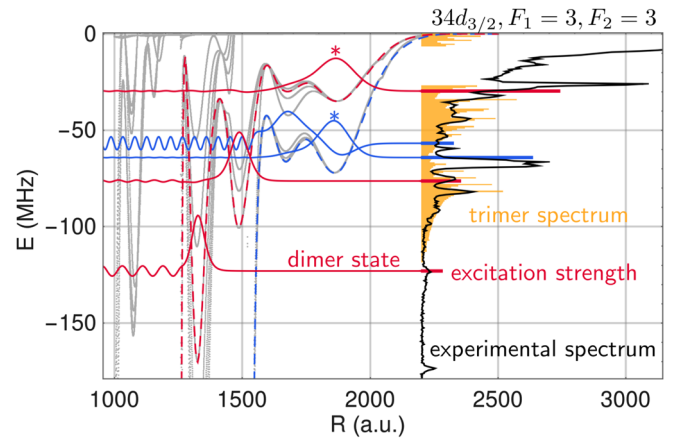


FIG. 2. Comparison between the experimental spectrum (black line) and theoretical results for molecules close to the Cs($34d_{3/2}$) $F_1 = F_2 = 3$ dissociation energy. Vibrational wave functions (colored full lines) are presented for a few diatomic potential curves (dashed lines) that have been selected from all potential energy curves (gray background). The offset of the wave function corresponds to its vibrational energy. The lengths of the colored bars on top of the experimental spectrum are the theoretical line strengths. The computed trimer histogram (bin width 700 kHz) is superimposed in orange. Dimer states localized in the most outer wells are marked with a star.

normalization $\mathcal{N}_{\pm}(\mathbf{R}_1, \mathbf{R}_2)$ and Rydberg wave functions $\phi_{n,l=2,m}(\mathbf{r})$. The corresponding angular potentials are

$$E_{\pm}(R, \theta) = E_{\text{dim}}(R) \left[1 \pm \left(-\frac{1}{2} + \frac{3}{2} \cos^2 \theta \right) \right], \quad (2)$$

where $E_{\text{dim}}(R)$ is the corresponding diatomic PES.

This result is illustrated in Fig. 1(a). The equilibrium angles are $\theta = 0$ and $\theta = \pi$ for E_+ and $\theta = \pi/2$ for E_- . These angles are energetically favored since the electronic wave function maximizes its density on the two ground state atoms in those configurations; see Fig. 1(b). The minima in the E_+ channel give twice the binding energy of the dimer state and this is the case that has thus far been discussed in formation of bound Rydberg trimers. The minimum of the E_- channel in the perpendicular configuration ($\theta = \pi/2$) is particularly interesting because it is not a global minimum, but yet can support vibrational states at $3/2$ the dimer binding energy. The above two-state model serves to highlight an essential finding of this work, namely the prediction of angular Rydberg trimer states in the E_- channel detuned to the red of the $\text{Cs}(nd_{3/2})$ thresholds.

We next turn on the relativistic spin mixing interactions for the Rydberg electron and the two ground state atoms. Relevant is the spin-orbit coupling $\mathbf{j} = \mathbf{s}_r + \mathbf{l}$, where \mathbf{l} is the angular momentum of the Rydberg electron, as well as the hyperfine coupling $\mathbf{F}_i = \mathbf{I}_i + \mathbf{s}_i$ for each perturber ($i = 1, 2$). The nuclear spin I of Cs is $7/2$. As for the diatomic case, these interactions couple the different spin channels of the contact interaction in (1) and lift the E_{\pm} degeneracy. This gives rise to the BO angular potential energy curves in Fig. 1(c). Like in the simple two-state picture one finds a first set of shallower E_- -type curves with minima at $\theta = \pi/2$ and a second set of deeper E_+ -type curves with minima at $\theta = 0$ and $\theta = \pi$.

These PES demonstrate that the Rydberg electron mediates an effective three-body force between the three atomic cores. The range of this interaction is on the order of the Rydberg orbit. A detailed analysis of the transition from Fig. 1(a)–1(c), where we trace back certain features of the angular structure to certain types of spin interactions, is performed in [35].

The experiments were performed in a crossed far-off resonance trap (FORT). The maximum number density of the FORT is $\sim 1 \times 10^{13} \text{ cm}^{-3}$ at a temperature of $\sim 40 \text{ } \mu\text{K}$. The photoassociation of the nd Rydberg molecules is achieved using a two-photon transition. Cs atoms are excited from the ground state, $6s_{1/2}(F=3)$, to Rydberg states using a near resonant transition to $6p_{3/2}(F=4)$ at 852 nm. This first step of the excitation is detuned from resonance by 300 MHz. For some experiments, where the resolution was $\sim 3 \text{ MHz}$, the laser that drives the first step of the transition is locked to a Cs saturated absorption setup and the Rydberg excitation laser at $\sim 508 \text{ nm}$ is locked to a Fabry-Pérot cavity. For the higher resolution experiments,

$\sim 700 \text{ kHz}$, both lasers were simultaneously locked to an ultrastable Fabry-Pérot cavity. Both lasers are linearly polarized in the same direction. The overall stability of the laser systems for the $\text{Cs}(34d_{3/2})$ and $\text{Cs}(36d_{3/2})$ measurements is $\sim 700 \text{ kHz}$ and $\sim 3 \text{ MHz}$, respectively. A signal is generated by ionizing the Rydberg atoms and projecting them onto a microchannel plate (MCP) detector in a time-of-flight spectrometer. The signal is collected as a function of laser detuning. Each prepared sample is excited with a series of laser pulses for a time of 150 ms, which amounts to 300 cycles of the excitation sequence. Each excitation pulse lasts $30 \text{ } \mu\text{s}$ and is followed by a 67 V cm^{-1} electric field pulse that lasts for 500 ns. Rydberg molecules can produce both Cs^+ ions and Cs_2^+ ions. For the $\text{Cs}(36d_{3/2})$ measurements we observe only the Cs^+ ions, whereas, for the $\text{Cs}(34d_{3/2})$ measurements, a better signal to noise ratio is achieved by observing both, Cs^+ and Cs_2^+ . The resulting spectra are presented in Figs. 2 and 3. Background electric fields in the experimental apparatus were measured to be 15 mV cm^{-1} .

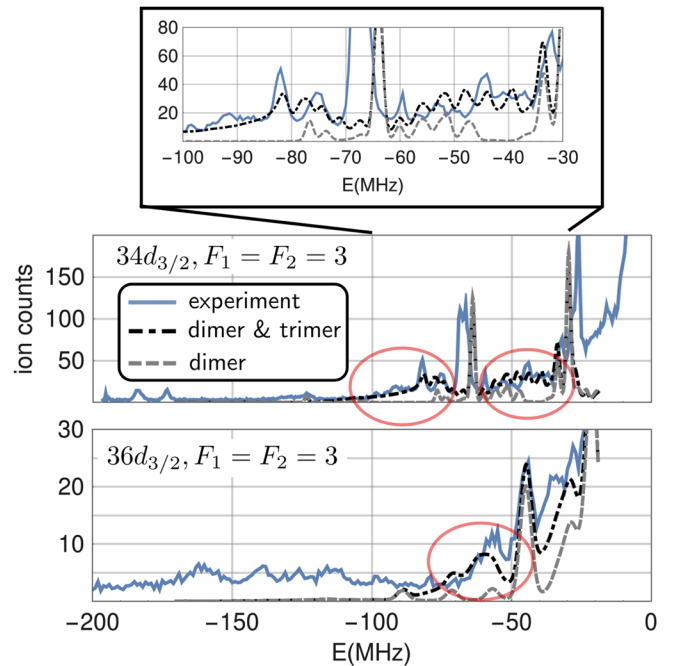


FIG. 3. Comparison of the experimental spectra (solid blue lines) and theoretical simulations including molecular dimer and trimer signals (dashed dotted black lines) close to the $\text{Cs}(34d_{3/2})$ and $\text{Cs}(36d_{3/2})$ atomic Rydberg lines with $F_1 = F_2 = 3$. To estimate the impact of trimer signals we also present theoretical simulations including only dimer states (dashed gray lines). The red circles highlight the energy regions where the contributions of the nonadditive trimers are most prominent in signal height and energy spread. The asymmetric long shoulders of these peaks can be explained only by the nonadditive trimer signals. The upper panel displays a magnification of the region with dominant trimer contributions for $34d_{3/2}$.

To compare our electronic structure calculations with experimentally observed spectra, we follow two complementary approaches for dimer and trimer states. For the Rydberg dimers, we compute vibrational wave functions $\chi_\nu(R)$; see Fig. 2 for the $34d_{3/2}$ excitation, with a finite difference method. The calculation yields bound states, including those bound by quantum reflection from steep potential drops [14]. To estimate the line strengths Γ_ν , we compute the Franck-Condon factors as $\Gamma_\nu \propto |\int dR \chi_0(R) R^2 \chi_\nu(R)|^2$, where the initial state $\chi_0(R)$ is the pair wave function for two ultracold atoms in the ground state, here a constant [38].

Calculated dimer states (colored full lines) are presented in Fig. 2 together with their line strengths (length of the colored horizontal bars) and are compared with the observed spectrum (black line). For ease of readability, we present only the most prominent dimer states with relatively large line strengths from a subset of potential curves (colored dashed curves), selected from all BO potentials (remaining gray curves). Since the line strength scales approximately quadratically with the bond length, the states in the most outer wells dominate the spectrum. In Fig. 2 these states are marked by stars and can be clearly identified with the strongest molecular lines in the experiment.

In a more detailed analysis, we use the computed dimer states as an input for a simulation of the dimer spectrum. The set of dimer states comprises not only those shown in Fig. 2 but all of the dimer states from the BO potentials that connect to the $34d_{3/2}$ atomic asymptote, independent of the strength of their Franck-Condon factors. In accordance with the experimental parameters, we generate these spectra by convoluting the discrete line strengths with Gaussian profiles having a width of 700 kHz (3 MHz) for $34d_{3/2}$ ($36d_{3/2}$). These simulations are presented in Fig. 3 (gray dashed lines) and are compared to the experimental signals (solid blue lines). The agreement of the line strengths and profiles is reasonable. However, some prominent spectral features are not captured with the dimer calculations, e.g., the broad peaks near the 45 and 80 MHz detuning in the Cs($34d_{3/2}$) spectrum (red circles). We show below that these features can *only* be explained with the addition of nonadditive trimer states, demonstrating the existence and observation of an effective three-body interaction in the formation of trimer molecules.

Because the density of angular states in the Rydberg molecules is large, we use a sampling technique to obtain line profiles of trimer states. This differs from the method used in Ref. [37]. Our approach is motivated by the fact that the trimer spectrum is dominated by signals from molecules where both ground state atoms are in the most outer wells, e.g., $R_1 = R_2 = 1868 a_0$ for $34d_{3/2}$, and that the experimental laser linewidth is larger than the spacing of bending excitations. Experimental signals of trimers with shorter bond lengths are suppressed, since the probability to find

two ground state atoms at distances R_1 and R_2 from the Rydberg atom scales as $(R_1 R_2)^2$. The trimer signal is then obtained as a histogram of energies $E(R_1, R_2, \theta)$, generated by drawing random molecular configurations with fixed $R_1 = R_2$ and variable θ . For $34d_{3/2}$ ($36d_{3/2}$) we use $R_1 = R_2 = 1868 a_0$ ($R_1 = R_2 = 2110 a_0$) and adjust the bin width to the 700 kHz (3 MHz) spectroscopic resolution. Furthermore we assume that the relative distribution of the atoms is isotropic (which implies a $\sin\theta$ distribution for the sampling) and take into account all the energy surfaces shown in Fig. 1(c). Hence, large contributions in the histogram are expected for energies close to $E(R_1, R_2, \theta \approx \pi/2)$, for stationary points in the PES, or for energetic regions where the PES are very dense. Since the molecule is frozen in a rigid rotor approximation to its radial equilibrium position, we account for the zero-point vibrational motion by blue-shifting the resulting histograms by 25 MHz (15 MHz) for $34d_{3/2}$ ($36d_{3/2}$). This sampling approach can be viewed as a modification of methods presented in [7] that were successfully applied to describe the spectrum of polyatomic ULRM in s -states. The resulting histogram for $34d_{3/2}$ is displayed in orange in Fig. 2 in comparison with the observed signal (for $32d_{3/2}$, $36d_{3/2}$, and $38d_{3/2}$, see [35]). Many characteristics of the shape of the histograms (such as the relative heights and the asymmetry of the peaks) agree with the observations. Because of the anisotropy of the PES, the energies of the simulated trimers cannot be obtained by addition of dimer energies. For $34d_{3/2}$ the corresponding dimer states that localize at $R = 1868 a_0$ are marked with a star in Fig. 2.

With the relatively high atomic density, we expect the experimental spectrum to contain both dimer and trimer signals. With this in mind, Fig. 3 shows the combined theoretical dimer and trimer spectrum (dot-dashed black curves) compared to experimental spectra (solid blue curves). The trimer signals are obtained by convoluting the histograms with Gaussian profiles having a width of 700 kHz for $34d_{3/2}$ and 3 MHz for $36d_{3/2}$. We normalize them to observed signals. The addition of the trimer lines significantly improves agreement with the observed data. The broad peaks near 45 and 80 MHz detuning in the $34d_{3/2}$ spectrum illustrate the presence of nonadditive trimer states where dimer lines are nearly absent. A similar trimer peak can be identified in the $36d_{3/2}$ spectrum; see the red circle in Fig. 3. Furthermore the higher resolution data for $34d_{3/2}$ reveal substructures in the trimer peaks (upper panel in Fig. 3) that are also predicted by our simulations and can be related to the energy spacing of the PES of approximately 4 MHz visible in Fig. 1(c), which is only resolved at sufficiently small line widths. The additional structures seen in the experimental spectra below -100 MHz might be due to the presence of radial trimers associated to inner wells

seen in Fig. 2. These states are influenced by the presence of the p -wave resonances and are not captured in our theory of three-body interactions.

We demonstrate that an effective three-body interaction can be realized by Rydberg excitation into anisotropic trimer ultralong-range molecules in an ultracold Cs gas. By including relativistic spin-dependent interactions in the Rydberg molecule Hamiltonian, we systematically analyze and identify observed spectroscopic features, as angular trimer Rydberg molecules whose energies are *not* multiples of dimer energies. Spectral features of radial dimers also are found and interpreted with accuracy. In the future, electric or magnetic fields can be employed to resolve and identify individual molecular lines due to the effective three-body terms. An interesting question that might be answered with an increased accuracy is whether the van der Waals interaction between the ground state atoms can have measurable effects for molecular trimers.

C. F. gratefully acknowledges a scholarship by the Studienstiftung des deutschen Volkes. P. S. acknowledges support from the Deutsche Forschungsgemeinschaft (DFG) within the Schwerpunktprogramm Giant Interactions in Rydberg Systems (GiRyd). J. Y., F. M., M. B., and J. P. S. acknowledge support from NSF Grant No. PHY-1607296. S. T. R. acknowledges support from NSF Grant No. PHY-1516421 and funding from the Research Corporation for Science Advancement. J. Y. lead the experimental effort. C. F. thanks T. Pfau, R. Löw, and F. Meinert for fruitful discussions.

-
- [1] C. H. Greene, A. S. Dickinson, and H. R. Sadeghpour, *Phys. Rev. Lett.* **85**, 2458 (2000).
- [2] V. Bendkowsky, B. Butscher, J. Nipper, J. P. Shaffer, R. Löw, and T. Pfau, *Nature (London)* **458**, 1005 (2009).
- [3] J. P. Shaffer, S. T. Rittenhouse, and H. R. Sadeghpour, *Nat. Commun.* **9**, 1965 (2018).
- [4] D. Booth, S. T. Rittenhouse, J. Yang, H. R. Sadeghpour, and J. P. Shaffer, *Science* **348**, 99 (2015).
- [5] A. Gaj, A. T. Krupp, J. B. Balewski, R. Löw, S. Hofferberth, and T. Pfau, *Nat. Commun.* **5**, 4546 (2014).
- [6] J. B. Balewski, A. T. Krupp, A. Gaj, D. Peter, H. P. Büchler, R. Löw, S. Hofferberth, and T. Pfau, *Nature (London)* **502**, 664 (2013).
- [7] M. Schlagmüller, T. C. Liebisch, H. Nguyen, G. Lohead, F. Engel, F. Böttcher, K. M. Westphal, K. S. Kleinbach, R. Löw, S. Hofferberth, T. Pfau, J. Pérez-Ríos, and C. H. Greene, *Phys. Rev. Lett.* **116**, 053001 (2016).
- [8] M. Schlagmüller, T. C. Liebisch, F. Engel, K. S. Kleinbach, F. Böttcher, U. Hermann, K. M. Westphal, A. Gaj, R. Löw, S. Hofferberth, T. Pfau, J. Pérez-Ríos, and C. H. Greene, *Phys. Rev. X* **6**, 031020 (2016).
- [9] M. T. Eiles, J. Pérez-Ríos, F. Robicheaux, and C. H. Greene, *J. Phys. B* **49**, 114005 (2016).
- [10] F. Camargo, R. Schmidt, J. D. Whalen, R. Ding, G. Woehl, S. Yoshida, J. Burgdörfer, F. B. Dunning, H. R. Sadeghpour, E. Demler, and T. C. Killian, *Phys. Rev. Lett.* **120**, 083401 (2018).
- [11] P. J. J. Luukko and J. M. Rost, *Phys. Rev. Lett.* **119**, 203001 (2017).
- [12] I. C. H. Liu and J. M. Rost, *Eur. Phys. J. D* **40**, 65 (2006).
- [13] I. C. H. Liu, J. Stanojevic, and J. M. Rost, *Phys. Rev. Lett.* **102**, 173001 (2009).
- [14] V. Bendkowsky, B. Butscher, J. Nipper, J. B. Balewski, J. P. Shaffer, R. Löw, T. Pfau, W. Li, J. Stanojevic, T. Pohl, and J. M. Rost, *Phys. Rev. Lett.* **105**, 163201 (2010).
- [15] F. Camargo, J. D. Whalen, R. Ding, H. R. Sadeghpour, S. Yoshida, J. Burgdörfer, F. B. Dunning, and T. C. Killian, *Phys. Rev. A* **93**, 022702 (2016).
- [16] J. Higgins, W. E. Ernst, C. Callegari, J. Reho, K. K. Lehmann, G. Scoles, and M. Gutowski, *Phys. Rev. Lett.* **77**, 4532 (1996).
- [17] A. Kitaev, *Ann. Phys. (Amsterdam)* **303**, 2 (2003).
- [18] D. Aharonov, W. van Dam, J. Kempe, Z. Landau, S. Lloyd, and O. Regev, *SIAM J. Comput.* **37**, 166 (2007).
- [19] J. Kempe, A. Kitaev, and O. Regev, *SIAM J. Comput.* **35**, 1070 (2006).
- [20] H. P. Büchler, A. Micheli, and P. Zoller, *Nat. Phys.* **3**, 726 (2007).
- [21] D. S. Petrov, *Phys. Rev. Lett.* **112**, 103201 (2014).
- [22] A. J. Daley and J. Simon, *Phys. Rev. A* **89**, 053619 (2014).
- [23] M. Hafezi, P. Adhikari, and J. M. Taylor, *Phys. Rev. B* **90**, 060503 (2014).
- [24] R. Faoro, B. Pelle, A. Zuliani, P. Cheinet, E. Arimondo, and P. Pillet, *Nat. Commun.* **6**, 8173 (2015).
- [25] D. B. Tretyakov, I. I. Beterov, E. A. Yakshina, V. M. Entin, I. I. Ryabtsev, P. Cheinet, and P. Pillet, *Phys. Rev. Lett.* **119**, 173402 (2017).
- [26] E. Fermi, *Il Nuovo Cimento* **11**, 157 (1934).
- [27] D. A. Anderson, S. A. Miller, and G. Raithel, *Phys. Rev. A* **90**, 062518 (2014).
- [28] D. A. Anderson, S. A. Miller, and G. Raithel, *Phys. Rev. Lett.* **112**, 163201 (2014).
- [29] S. Markson, S. T. Rittenhouse, R. Schmidt, J. P. Shaffer, and H. R. Sadeghpour, *Chem. Phys. Chem.* **17**, 3683 (2016).
- [30] H. Saßmannshausen, F. Merkt, and J. Deiglmayr, *Phys. Rev. Lett.* **114**, 133201 (2015).
- [31] F. Böttcher, A. Gaj, K. M. Westphal, M. Schlagmüller, K. S. Kleinbach, R. Löw, T. C. Liebisch, T. Pfau, and S. Hofferberth, *Phys. Rev. A* **93**, 032512 (2016).
- [32] E. L. Hamilton, C. H. Greene, and H. R. Sadeghpour, *J. Phys. B* **35**, L199 (2002).
- [33] A. A. Khuskivadze, M. I. Chibisov, and I. I. Fabrikant, *Phys. Rev. A* **66**, 042709 (2002).
- [34] M. T. Eiles and C. H. Greene, *Phys. Rev. A* **95**, 042515 (2017).
- [35] See Supplemental Material at <http://link.aps.org/supplemental/10.1103/PhysRevLett.122.103001> for further details on the experiment and the theoretical description of dimer and trimer states.
- [36] C. Fey, F. Hummel, and P. Schmelcher, *Phys. Rev. A* **99**, 022506 (2019).
- [37] C. Fey, M. Kurz, and P. Schmelcher, *Phys. Rev. A* **94**, 012516 (2016).
- [38] B. J. DeSalvo, J. A. Aman, F. B. Dunning, T. C. Killian, H. R. Sadeghpour, S. Yoshida, and J. Burgdörfer, *Phys. Rev. A* **92**, 031403 (2015).